

Model Calculations and Interferometer Measurements of Ice Cloud Characteristics

Sunggi Chung¹, Steven Ackerman¹, Paul F. van Delst¹, and W. Paul Menzel²

¹ Cooperative Institute for Meteorological Satellite Studies,

University of Wisconsin – Madison

² NOAA/NESDIS

Office of Research and Applications

Madison, Wisconsin

Submitted August 1998

Corresponding author address:

Dr. Sunggi Chung

University of Wisconsin-Madison

1150 University Ave

Madison, WI 53706

Phone: 608-262-7476

Fax: 608-262-3077

Email: schung4@facstaff.wisc.edu

Abstract

This paper investigates the relationship between high-spectral resolution infrared (IR) radiances and the microphysical and macrophysical properties of cirrus clouds. Using radiosonde measurements of the atmospheric state at the Department of Energy's Atmospheric Radiation Measurement (ARM)-site, high-spectral resolution IR radiances are calculated by combining trace gas absorption optical depths from a line-by-line radiative transfer model with the discrete ordinate radiative transfer (DISORT) model. The sensitivity of the high-spectral resolution IR radiances to particle size, ice water path, cloud top location, cloud thickness, and multi-layered cloud conditions is estimated in a multitude of calculations.

DISORT calculations and interferometer measurements of cirrus ice cloud between 700 and 1300 cm^{-1} are compared for three different situations. The measurements were made with the High-spectral resolution Interferometer Sounder (HIS) mounted on NASA ER-2 aircraft flying at 20 km during the SUBsonic aircraft Contrail and Cloud Effects Special Study (SUCCESS).

1. Introduction

The importance of cirrus to the earth radiation budget is well established (Stephens and Webster 1981; Liou 1986). To improve the representation of cirrus in climate models, global distributions of cirrus ice water content and crystal size are required. Satellite observations are needed to satisfy this global requirement. Satellite instruments that measure the infrared (IR) radiance at high-spectral resolution show promise for improving the capability of characterizing ice clouds globally. In the next several years, the Atmospheric Infrared Radiation Sounder (AIRS) on the Earth Observing System - PM platform in 2002 and the Infrared Atmospheric Sounding Interferometer (IASI) on the Meteorological Operational Platform (METOP) in 2003 will place high spectral resolution infrared sounders into polar orbit. Cirrus ice particle size and ice water paths can be inferred so that the effect of these clouds on the Earth radiation budget will be more fully understood.

Algorithms for retrieving cirrus properties have been developed and applied to HIS measurements by Ackerman et al. 1990, Smith et al. 1993, and Smith et al. 1998. The cloud parameters are inferred by minimizing the difference between theoretical calculations and the interferometer observations. The accuracy of the retrieved effective microphysical properties is fundamentally tied to accurate specification of the cloud boundaries. In the referenced studies, cloud boundaries were specified with lidar measurements. In the absence of a lidar, a single cloud effective altitude is assigned using the CO₂ slicing method (Smith and Frey 1990).

This paper presents the procedure for calculating emitted spectra of ice clouds in Section 2. The sensitivity of high-spectral resolution IR observations to cirrus cloud microphysical and macrophysical properties with simulated data sets is investigated in Section 3. Particle size and ice water path are explored in Sections 3.a and 3.b respectively. Section 3.c investigates the sensitivity of

high-spectral resolution measurements to cloud property retrieval in the presence of errors in cloud boundary assignment. Simulations showing the errors associated with retrievals under multi-layered cloud conditions are presented in Section 3.d. Section 3.e describes simulations assessing the sensitivity of the high-spectral resolution measurements to vertical variations in cloud particle size.

Actual measurements from the High-spectral resolution Interferometer Sounder (HIS) are presented in Section 4 and effective particle size and ice water path are retrieved. Conclusions are made in Section 5.

2. Calculation of Emitted Spectra for Ice Clouds

The differential equation for radiative transfer is well known (Chandrasekhar 1960; Stamnes et al. 1988; Tsay et al. 1990). Using the algorithm of Stamnes et al. (1988),

$$\mathbf{m} \frac{du_n(\mathbf{t}_n, \mathbf{m}, \mathbf{f})}{d\mathbf{t}} = u_n(\mathbf{t}_n, \mathbf{m}, \mathbf{f}) - S_n(\mathbf{t}_n, \mathbf{m}, \mathbf{f}), \quad (1)$$

where $u_n(\mathbf{t}_n, \mathbf{m}, \mathbf{f})$ is the (specific) intensity of monochromatic frequency n in the plane-parallel layer of optical depth \mathbf{t}_n in the direction of (\mathbf{m}, \mathbf{f}) . Here, \mathbf{f} is the azimuthal angle and \mathbf{m} is the cosine of the zenith angle. The source function S_n consists of

$$S_n(\mathbf{t}_n, \mathbf{m}, \mathbf{f}) = \frac{w_n(\mathbf{t}_n)}{4\pi} \int_0^{2\pi} d\mathbf{f}' \int_{-1}^1 d\mathbf{m}' P_n(\mathbf{t}_n, \mathbf{m}, \mathbf{f}; \mathbf{m}', \mathbf{f}') u_n(\mathbf{t}_n, \mathbf{m}', \mathbf{f}') + Q_n(\mathbf{t}_n, \mathbf{m}, \mathbf{f}), \quad (2)$$

where w_n is the single scattering albedo and $P_n(\mathbf{t}_n, \mathbf{m}, \mathbf{f}; \mathbf{m}', \mathbf{f}')$ is the phase function. The first term is due to the multiple scattering. The second term is due to the internal source and is generally written as

$$Q_n(\mathbf{t}_n, \mathbf{m}, \mathbf{f}) = Q_n^{(thermal)}(\mathbf{t}_n, \mathbf{m}, \mathbf{f}) + Q_n^{(beam)}(\mathbf{t}_n, \mathbf{m}, \mathbf{f}), \quad (3)$$

$$Q_n^{(thermal)}(\mathbf{t}_n, \mathbf{m}, \mathbf{f}) = [1 - w_n(\mathbf{t}_n)] B_n [T] \quad (4)$$

$$Q_n^{(beam)}(\mathbf{t}_n, \mathbf{m}, \mathbf{f}) = \frac{w_n(\mathbf{t}_n)}{4p} I^{inc} P_n(\mathbf{t}_n, \mathbf{m}, \mathbf{f}; -\mathbf{m}_0, \mathbf{f}_0) \exp(-\mathbf{t}_n / \mathbf{m}_0), \quad (5)$$

where $B_n[T]$ is the Planck function at temperature T , and $Q_n^{(beam)}$ arises due to the usual distinction of direct-diffuse radiation, \mathbf{m}^{inc} being the incident flux.

To arrive at the Discrete-Ordinate-Method Radiative Transfer (DISORT), the scattering phase function is expanded by the Legendre polynomials as

$$P(\mathbf{t}_n, \cos \Theta) = \sum_{\ell=0}^{2N-1} (2\ell + 1) g_\ell(\mathbf{t}_n) P_\ell(\cos \Theta), \quad (6)$$

where

$$\cos \Theta = \mathbf{m}\mathbf{m}' + \sqrt{(1 - \mathbf{m}^2)(1 - \mathbf{m}'^2)} \cos(\mathbf{f} - \mathbf{f}'). \quad (7)$$

Accordingly, the intensity function is expanded as

$$u_n(\mathbf{t}_n, \mathbf{m}, \mathbf{f}) = \sum_{m=0}^{2N-1} u_n^m(\mathbf{t}_n, \mathbf{m}) \cos m(\mathbf{f}_0 - \mathbf{f}). \quad (8)$$

In this work, the solution for Eq. (1) is found one wavenumber at a time from 700.0 to 1300.0 cm^{-1} in steps of 0.1 cm^{-1} using the DISORT algorithm of Stamnes et al. 1988. The number of expansion terms $2N$ in Eqs. (6) and (8) is relevant to the accuracy of the numerical integration by Gaussian quadrature. Calculations with $N=16, 24$, and 32 produce results within 0.02% in the entire range of 700 to 1300 cm^{-1} , so $N=24$ was adopted. Contributions to the source function $Q_n^{(beam)}$ in Eq. (3) from the sun are presumed to be insignificant in the infrared range between 700 and 1300 cm^{-1} and are ignored. The phase function is approximated by the Henyey-Greenstein function so that $g_\ell(\mathbf{t}_n)$ in Eq. (6) is replaced by the $\ell - th$ power of the asymmetry factor, that is,

$$g_\ell(\mathbf{t}_n) = g_{Asym}^\ell(\mathbf{t}_n). \quad (9)$$

The extinction coefficient (and hence t_n), the single-scattering albedo w_n , and the asymmetry factor $g_{Asym}(t_n)$ are computed from Mie calculations for various clouds, assuming a Deirmendjian type distribution function (Deirmendjian, 1964),

$$n(r) = ar^a \exp(-br). \quad (10)$$

If the peak of the distribution function occurs at r_c , then

$$b = a / r_c. \quad (11a)$$

In this work, α is chosen to be 6. The normalization constant is given by

$$a = \left(\frac{a}{r_c}\right)^{(a+1)} / (a!). \quad (11b)$$

The particle size is assumed to be spherical and is measured in terms of the effective radius, defined as

$$r_{eff} = \frac{\int_0^{\infty} n(r)r^3 dr}{\int_0^{\infty} n(r)r^2 dr}. \quad (12)$$

The atmospheric temperature, pressure, and relative humidity as a function of the altitude are inferred from radiosondes launched from the DOE Atmospheric Radiation Measurement (ARM) site. The clear sky optical depths are computed as the integral sum of the absorption by H₂O and other atmospheric molecules using LBLRTM (Line-By-Line Radiative Transfer Model) (Clough et al. 1992). The atmosphere (0.315 - 20.0 km) is divided into 56 layers so that the temperature difference across any boundary is no greater than 3.5K. The theoretical calculations of spectra in ice cloud situations are performed using the Discrete-Ordinate Radiative Transfer (DISORT) method (Stamnes et al. 1988).

3. Sensitivity Studies

The vertical distributions of particle effective size (r_{eff}) and the ice-water path (IWP) are important cirrus microphysical properties for radiative transfer. The cloud top and base altitudes are also important as they define the cloud effective temperature. The shape of the ice crystals composing the cirrus is thought to be a secondary effect in the IR region (Takano et al. 1992). This section presents the influence of these characteristic parameters on cloud forcing, defined as the difference of upwelling radiance of the clear and cloudy skies, expressed in brightness temperature.

a. Ice-Particle Size (r_{eff})

Variations in the cloud forcing spectra, resulting from a cirrus cloud composed of a uniform particle size distribution, were investigated for effective particle sizes, r_{eff} , ranging from 4.5 to 22.5 μm . The DISORT calculation was performed for a 0.8 km thick cloud layer at an altitude of 10.8 km with an IWP of 10.0 gm^{-2} . Fig. 1a shows the variation of the cloud forcing as a function of the effective radius r_{eff} . In the infrared window region between 800 and 900 cm^{-1} , the cloud forcing increases from 20 K for 22.5 μm ice particles to more than 65 K for 4.5 μm ice particles; the smaller particles cause more attenuation in the infrared window radiation for a fixed IWP. The spectral change in cloud forcing from 800 to 1000 cm^{-1} shows a pronounced S-shape for smaller ice particles (less than 10 μm) which becomes more linear for larger ice particles (greater than 10 μm). This S-shape was previously reported by Smith et al. (1998) for 7.5 μm ice particles. This characteristic shape of the spectral cloud forcing between 800 and 1000 cm^{-1} for small and large ice particles is useful for distinguishing the ice-particle size ranges of cirrus clouds. Between 1100 and 1200 cm^{-1} the cloud forcing increases from about 15 to 40 K with decreasing ice particle size, but there are no pronounced differences in the shape as r_{eff} changes. In fact in this range of wavenumbers, the cloud forcing is nearly constant as a function of

wavenumber. Fig 1b shows a companion plot to Fig 1a where the optical depth is kept constant (rather than the ice water path) and the ice particle size is varied. The same general characteristics of Fig 1a appear in this plot.

Three radiative parameters are affected by a change of effective radius r_{eff} - the optical depth t , albedo w , and asymmetry factor g_{Asym} . The interplay of these parameters within the radiative transfer equation is complex, but qualitatively the wavenumber region 800 to 1000 cm^{-1} is affected more by changes in t than by variations in w or g_{Asym} , whereas changes in all three parameters affect the 1100 to 1200 cm^{-1} region.

b. Ice-Water Path (IWP) and Cloud Opacity

The attenuation of radiation increases with increasing IWP and is wavenumber dependent. Fig. 2 shows the spectral variation of the cloud forcing as IWP changes but r_{eff} is fixed at 7.5 μm . Cloud forcing at 1000 cm^{-1} increases from about 20 to 75 K as IWP increases from 7 to 80 gm^{-2} ; the corresponding change at 800 cm^{-1} is 40 to 75 K. Large IWP renders the cloud opaque and the spectral cloud forcing becomes almost constant. The S-shape of the cloud forcing is clearly seen for IWP = 7.0 and 15.0 gm^{-2} , but is much less pronounced at IWP = 22.5 - 30.0 gm^{-2} . For IWP = 50.0 gm^{-2} the cloud forcing shows very little spectral dependence and the cloud appears to be opaque. In this paper a cloud is called opaque if the upwelling radiance is changed by less than one degree K as the underlying atmosphere changes. With this definition, clouds of $r_{eff} = 7.5, 15.0, \text{ and } 30.0 \mu\text{m}$ become opaque when the IWP exceeds about 45, 70, and 130 gm^{-2} respectively.

c. Cloud Altitude and Thickness

Difficulties in defining the cloud altitude increase the uncertainty in the retrieved cloud properties. To estimate the impact, a reference upwelling radiance was computed for a 1.1 km thick cloud ($r_{eff} =$

30 μm and $\text{IWP} = 20 \text{ gm}^{-2}$) at 11.1 km. The IWP was retrieved by minimizing the cloud forcing difference between the reference and the calculated spectra in the 700-1300 cm^{-1} region. The IWP retrievals assumed a known clear-sky spectrum, cloud thickness of 1 km, $r_{\text{eff}} = 30 \mu\text{m}$. Fig. 3 shows the error in the retrieved IWP as a function of the specified cloud top altitude. An uncertainty of 1 km in altitude leads to an IWP error of approximately 2 gm^{-2} (about 10%). As expected, assuming the cloud is too high results in a lower value for the retrieved IWP and thus more radiance from below the cloud is transmitted to match the simulated observation. Assuming the cloud altitude is too low results in a retrieved IWP that is too large. The error is a non-linear function with assumed cloud-top altitude; assuming the cloud is at 7.8 km increases the IWP error to 10 gm^{-2} (about 50%).

The sensitivity of the cloud forcing spectrum with respect to the cloud thickness was also investigated. For a given cloud top (13.1 km) and IWP (10.0 gm^{-2}), the cloud base altitude was varied from 12.1 to 6.6 km. Fig. 4 shows the cloud forcing spectrum as a function of the cloud base (or cloud thickness). A 1 km error in cloud thickness leads to a decrease of cloud forcing by about 1.5 K and 0.7 K in the wavenumber regions 800-1000 cm^{-1} and 1100-1200 cm^{-1} respectively. Compared to the sensitivity to particle size (see Fig. 1a), this indicates a relative insensitivity to the thickness of the cloud for fixed IWP.

d. Multi-layered Clouds

It is not unusual for a water cloud to exist below a cirrus cloud. To assess the IWP error caused by assuming a single layered cirrus in a multi-layered cloud condition, three sets of numerical experiments are undertaken. The upwelling radiances were computed for a 1.1 km cirrus layer ($r_{\text{eff}} = 7.5 \mu\text{m}$; $\text{IWP} = 10, 20, \text{ or } 40 \text{ gm}^{-2}$) at 11.1 km, with an underlying water cloud ($r_{\text{eff}} = 20 \mu\text{m}$; $\text{LWP} = 30 \text{ gm}^{-2}$) at altitudes ranging from 3.1 to 5.0 km. In each case, an IWP and r_{eff} were retrieved for an

isolated cirrus cloud (the water cloud is assumed to be undetected). The underlying cloud decreases the radiance at the cirrus cloud base and the retrieved cirrus IWP is always greater than the true value. Fig. 5 shows the increase in the retrieved cirrus IWP as a function of the altitude of the unseen water cloud below. Not surprisingly, thin cirrus ($IWP = 10 \text{ gm}^{-2}$) are more susceptible to changes in underlying conditions than thick cirrus ($IWP = 40 \text{ gm}^{-2}$); retrieved thin cirrus IWP range from 14.5 to 19.5 gm^{-2} while thick cirrus IWP range from 44 to 47 gm^{-2} . The unseen water cloud at 5.0 km causes a greater change in the cirrus IWP than the unseen water cloud at 3.1 km, since the 5.0 km cloud attenuates the radiation between 3.1 and 5.0 km but the 3.1 km cloud does not. Cirrus r_{eff} ranges from 9.6 to 10.875 μm , 8.625 to 9.375 μm , and 8.025 to 8.625 μm for the initial cirrus IWP of 10, 20, and 40 gm^{-2} , respectively.

e. Vertical Variations in Cloud Particle Size

Most passive IR retrieval methods assume the cloud microphysics is uniformly distributed within the cloud. This section investigates the sensitivity of the high-spectral radiances to the vertical structure of cloud particle size for constant IWP. The cloud is divided into two layers; the upper layer occupies 11.1 to 10.0 km and the lower layer from 10.0 to 8.9 km. One layer is composed of small particles ($r_{eff} = 9.0 \mu\text{m}$) and the other has large particles ($r_{eff} = 22.5 \mu\text{m}$); both layers have the same IWP (5 gm^{-2}). The cloud forcing of "small particle over large" and "large particle over small" is investigated. With the two layers placed at 10.0 and 11.1 km, calculations show that the cloud forcing by "small over large" is greater by 1-2 K than "large over small." Fig. 6 shows the cloud forcing from these two cloud configurations; the net cloud forcing is similar to that of an ice cloud of particle size around 13 μm . The thin cirrus cloud forcing is relatively insensitive to vertical variations in cloud particle size and is weighted toward the smaller particle size in average behavior.

4. Comparison with HIS Measurements

This section presents comparisons of theoretical calculations of cirrus ice cloud forcing and interferometer measurements between 700 and 1300 cm^{-1} for three different ice cloud situations. The upwelling radiance spectra were observed by the High spectral resolution Interferometer Sounder (HIS) mounted on a NASA ER-2 aircraft flying at 20 km during the SUBsonic aircraft Contrail and Cloud Effects Special Study (SUCCESS) on 21 April 1996 over the U.S. Great Southern Plains. The HIS is a Michelson interferometer with a spectral resolving power ($\lambda/\Delta\lambda$) of approximately 3000 covering the spectral range from 3.7-16.7 μm . The HIS spectra have an unapodized resolution of approximately 0.35 cm^{-1} from 600-1100 cm^{-1} , and 0.7 cm^{-1} resolution from 1100-2700 cm^{-1} . Integrated high emissivity, temperature controlled reference blackbodies are used for an absolute calibration. The HIS has a noise equivalent temperature and reproducibility of about 0.1-0.2 K over much of the spectrum. Revercomb et al. (1988) provide a detailed description of the instrument; Smith et al. (1998) report on the interferometer measurements from SUCCESS.

Data from SUCCESS clouds labeled as 963, 990, and 998 (from 20:24:50 UTC, 20:29:20 UTC, and 20:31:17 UTC respectively during the 21 April 1996 flight) were investigated. Cloud forcing was determined using the observed spectra for cloudy and clear sky observations; the time between the measurements of the clear and cloudy skies is less than 20 minutes.

The DISORT calculation relied on cloud altitude and thickness provided independently by the Cloud and aerosol LIDAR System (CLS) flying on the ER-2 aircraft (Spinhirne et al. 1996).

Atmospheric temperature, pressure, and relative humidity were measured with the ARM-site

radiosondes (Lesht 1995). Optical depths are calculated with LBLRTM and the extinction coefficients, single-scattering albedo, and asymmetry factor of the clouds are determined from Mie calculations.

SUCCESS Cloud 998, observed at 20:31:17 UTC on 21 April 1996, consists of two layers: one extends from 11.445 to 10.530 km (implying a thickness for the upper cloud of 0.915 km) and the other is found between 2.355 and 2.130 km (0.225 km thick). The effective radius and IWP are retrieved by matching the DISORT calculation to the HIS measurements. Close agreement between the HIS measurement and DISORT calculation is found to occur with an r_{eff} in the range of 7.2 to 7.7 μm and with IWP in the range of 6.6 to 7.1 gm^{-2} . The RMS (root mean square) differences of observed and calculated spectra are less than 1.5 K in 800-1000 cm^{-1} and 2.5 K in 1150-1250 cm^{-1} . Fig. 7 shows the HIS spectrum and the DISORT calculation with $r_{eff}=7.35 \mu\text{m}$ and $\text{IWP} = 6.85 \text{gm}^{-2}$. The unusual inverted "S" shape in 800-1000 cm^{-1} , characteristic of small-size particle cirrus clouds, is apparent.

SUCCESS cloud 990, observed at 20:29:20 UTC on 21 April 1996, is composed of layers at 10.515 to 9.690 km, 8.820 to 7.365, and 1.665 to 1.260 km. The best DISORT result is obtained with $r_{eff} = 37.5 \mu\text{m}$ and $\text{IWP} = 55.0 \text{gm}^{-2}$; RMS differences of observed and calculated spectra are 1.9K (800-1000 cm^{-1}) and 4.1K (1150-1250 cm^{-1}). Fig. 8 shows the comparison between the HIS observation and the DISORT calculation. The quality of the comparison of observed and calculated spectra does not change appreciably as r_{eff} changes by 10.0 μm and IWP changes by 10 g m^{-2} .

SUCCESS cloud 963, observed at 20:31:17 UTC on 21 April 1996, is reported to have three layers from 10.830 to 9.600 km, 9.255 to 7.950 km, and 7.575 to 7.305 km and calculations suggest $r_{eff} = 37.5 \mu\text{m}$ and $\text{IWP} = 604 \text{gm}^{-2}$; RMS differences are 1.8K (800-1000 cm^{-1}) and 4.5K (1150-1250 cm^{-1}). Both calculated and observed spectra are shown in Fig. 9. From these calculations, r_{eff} is estimated

within $10.0 \mu\text{m}$ and IWP within 50 gm^{-2} . These clouds are more opaque than SUCCESS cloud 998 and their spectral cloud forcing is nearly constant with wavenumber from 800 to 1000 cm^{-1} , indicative of larger ice particles. The assumption of a spherical shape for the ice particle might be suspect and thus interfering with a better fit of observed and calculated spectra.

5. Conclusions

Calculations of high-spectral resolution infrared radiances in cirrus cloud situations indicate that cloud forcing (clear minus cloudy) spectra are sensitive to ice particle size, ice water path, and cloud altitude. They are less sensitive to cloud thickness and lower layer clouds. These studies present the probable errors in cloud forcing when one or more of the cloud characteristics are not accurately known.

A numerical procedure based on the DISORT algorithm is used to retrieve the effective radius and ice water path of cloud layers with known optical depths and cloud boundaries and with nearby clear sky atmospheric conditions also known. The best sets of effective radius and ice water path can reproduce the observed HIS cloud forcing within 2 K in 800 - 1000 cm^{-1} and within 4.5 K in 1150 - 1250 cm^{-1} for both small ($r_{eff} < 10 \mu\text{m}$) and large ($r_{eff} > 10 \mu\text{m}$) particle clouds. Measured spectra from the HIS have been used to infer a range of ice particle sizes between 7.5 and $40 \mu\text{m}$ with ice water paths between 10 and 600 gm^{-2} . The reasonable reproduction in a rather wide window region suggests that the DISORT based algorithm can distinguish small from large particle clouds as well as provide a fair estimate of IWP. Ice particle size and ice water path are estimated with 20% variation in the inferred values.

Cirrus clouds with small ice particles ($r_{eff} < 10 \mu\text{m}$) exhibit a non-linear S-shaped cloud forcing in $800 - 1000 \text{ cm}^{-1}$ that gradually disappears as the particle size is increased. Clouds with ice water path (IWP) greater than 50 gm^{-2} (130 gm^{-2}) and small (large) particles of $r_{eff} = 7.5 \mu\text{m}$ ($r_{eff} = 30\mu\text{m}$) are found to be opaque (upwelling radiance is unchanged within 1 K).

Imagers with three or four broad band (spectral resolution around $10 - 20 \text{ cm}^{-1}$) measurements in the infrared window region between 800 to 1000 cm^{-1} are likely to be able to distinguish large from small particle size cirrus and to provide IWP estimates. Suitable applications may include detection and mapping of the global distribution of aircraft contrails as well as cirrus clouds. High spectral resolution sounders in polar orbit will be capable of characterizing both r_{eff} and IWP for ice clouds unambiguously.

References

- Ackerman, S. A., W. L. Smith, J. D. Spinhirne, and H. E. Revercomb, 1990: The 27-28 October 1986 FIRE IFO cirrus case study: Spectral properties of cirrus clouds in the $8-12 \mu\text{m}$ window. *Mon. Wea. Rev.*, **118**, 2377-2388.
- Chandrasekhar, S., 1960: *Radiative Transfer*. Dover Press, pp.
- Clough, S. A., M. J. Iacono, and J.-L. Moncet, 1992: Line-by-line calculation of atmospheric fluxes and cooling rates: Application to water vapor. *J. Geophys. Res.*, **97**, 15761-15785 .
- Deirmendjian, D., 1964: Scattering and polarization properties of water clouds and hazes in the visible and infrared. *Appl. Opt.*, **3**, 187-196.
- Lesht, B. M., 1995: An evaluation of ARM radiosonde operational performance. Proceedings of the Ninth Symposium on Meteorological Observations and Instrumentation American Meteorological Society, Boston, MA. pp. 6-10.

- Liou, K. N., 1986: Influence of cirrus clouds on weather and climate processes: A global perspective. *Mon. Wea. Rev.*, **114**, 1167-1199.
- Revercomb, H. E., H. Buijs, H. B. Howell, D. D. LaPorte, W. L. Smith, and L. A. Sromovsky, 1988: Radiometric calibration of IR Fourier transform spectrometers: Solution to a problem with the High spectral resolution Interferometer Sounder. *Appl. Opt.*, **27**, 3210-3218.
- Smith, W. L., S. Ackerman, H. Revercomb, H. Huang, D. H. DeSlover, W. Feltz, L. Gumley, and A. Collard, 1998: Infrared spectral absorption of nearly invisible cirrus clouds. *Geophys. Res. Lett.*, **25**, 1137-1140.
- Smith, W. L., and R. Frey, 1990: On cloud altitude determinations from High spectral resolution Interferometer Sounder (HIS) observations. *J. Appl. Meteor.*, **29**, 658-662.
- Smith, W. L., X. L. Ma, S. A. Ackerman, H. E. Revercomb, and R. O. Knuteson, 1993: Remote sensing cloud properties from high-spectral resolution infrared observations. *J. Atmos. Sci.*, **50**, 1708-1720.
- Spinhirne, J. D., W. D. Hart, and D. Hlavka, 1996: Cirrus infrared parameters and shortwave reflectance relations from observations. *J. Atmos. Sci.*, **53**, 1438-1458.
- Stamnes, K., S.-C. Tsay, W. Wiscombe, and K. Jayaweera 1988: A numerically stable algorithm for discrete-ordinate-method radiative transfer in multiple scattering and emitting layered media. *Appl. Opt.*, **27**, 2502-2509.
- Stephens, G. L. and P. J. Webster, 1981: Clouds and climate: Sensitivity of simple systems. *J. Atmos. Sci.*, **38**, 235-247.
- Takano, Y., K. N. Liou, and P. Minnis, 1992: The effects of small ice crystals on cirrus infrared radiative properties. *J. Atmos. Sci.*, **49**, 1487-1493.

Tsay, S-C., K. Stamnes, and K. Jayaweera, 1990: Radiative transfer in stratified atmospheres:

Development and verification of a unified model. *J. Quant. Spectrosc. Radiat. Transfer*, **43**, 133-148.

Acknowledgements

The authors gratefully acknowledge Drs. Wiscombe and Tsay for providing them with the computer code of DISORT. This work was funded by NASA grant NAS5-31367.

Figure Captions

Figure 1a. The sensitivity of high spectral resolution observations to variations in cloud effective radius. Cloud forcing represents the brightness temperature difference between a clear and a cloudy sky calculation. Eight different effective radii are assumed, they are (from the top curve to the bottom) 4.5, 6.0, 7.5, 9.0, 12.0, 15.0, 18.75, and 22.5 μm . The cloud has a constant IWP of 10 g m^{-2} and a cloud top altitude of 10.8 km.

Figure 1b. The sensitivity of high spectral resolution observations to variations in cloud particle effective radius. Cloud forcing represents the brightness temperature difference between a clear and a cloudy sky calculation. Six different effective radii are assumed, they are (from the top curve to the bottom) 4.5, 6.0, 7.5, 9.0, 12.0, and 18.75 μm . The cloud has a constant optical depth at 1000 cm^{-1} of 0.5 and the cloud top altitude is 10.8 km.

Figure 2. Cloud forcing as a function of wavenumber for 5 different IWP: 50, 30, 22.5, 15 and 7.0 g m^{-2} (from top to bottom). The clouds have the same r_{eff} of $7.5 \mu\text{m}$, a cloud top altitude of 10.8 km, and a thickness of 0.8 km.

Figure 3. Errors in retrieved IWP if the cloud-top altitude is incorrectly assigned during the retrieval. The ice cloud has an IWP of 20 g m^{-2} , an effective radius of $30 \mu\text{m}$ and exists between 11.1 and 10.0 km.

Figure 4. Cloud forcing as a function of wavenumber for different cloud base altitudes of 12.1, 11.1, 10.0, 8.9 and 7.8 and 6.6 km (from top to bottom). The cloud has a constant IWP of 10 g m^{-2} and an effective radius of $10.5 \mu\text{m}$; the cloud top altitude is 13.1 km.

Figure 5. Errors in retrieved IWP for a multi-layered cloud condition, if a single 1 km cloud layer is assumed. The cirrus cloud has an effective radius of $7.5 \mu\text{m}$ and is between 11.1 and 10.0 km. The lower water cloud is approximately 1 km thick at altitudes ranging from 3.1 to 5.0 km and has an LWP of 30 g m^{-2} and an effective particle radius of $20 \mu\text{m}$. The retrieved errors are shown for three cirrus IWP conditions, 40, 20, and 10 g m^{-2} .

Figure 6. The sensitivity of high spectral resolution observations to variations in the vertical distribution of effective radius. In the top curve the upper cloud layer has an effective particle radius of $9.0 \mu\text{m}$ and the lower has an effective particle radius of $22.5 \mu\text{m}$. The particle sizes are reversed in the lower curve. Cloud forcing represents the brightness temperature difference between a clear and a cloudy sky calculation. The cloud has a constant IWP of 10 g m^{-2} and lies between 11.1 and 8.9 km.

Figure 7. Cloud forcing as a function of wavenumber for a HIS observed spectrum during the SUCCESS experiment and results from a DISORT calculation with an effective radius of $7.35 \mu\text{m}$ and an IWP of 6.85 g m^{-2} .

Figure 8. Cloud forcing as a function of wavenumber for a HIS observed spectrum during the SUCCESS experiment and results from a DISORT calculation with an effective radius of $37.5 \mu\text{m}$ and an IWP of 55 g m^{-2} .

Figure 9. Cloud forcing as a function of wavenumber for a HIS observed spectrum during the SUCCESS experiment and results from a DISORT calculation with an effective radius of $37.5 \mu\text{m}$ and an IWP of 604 g m^{-2} .

a

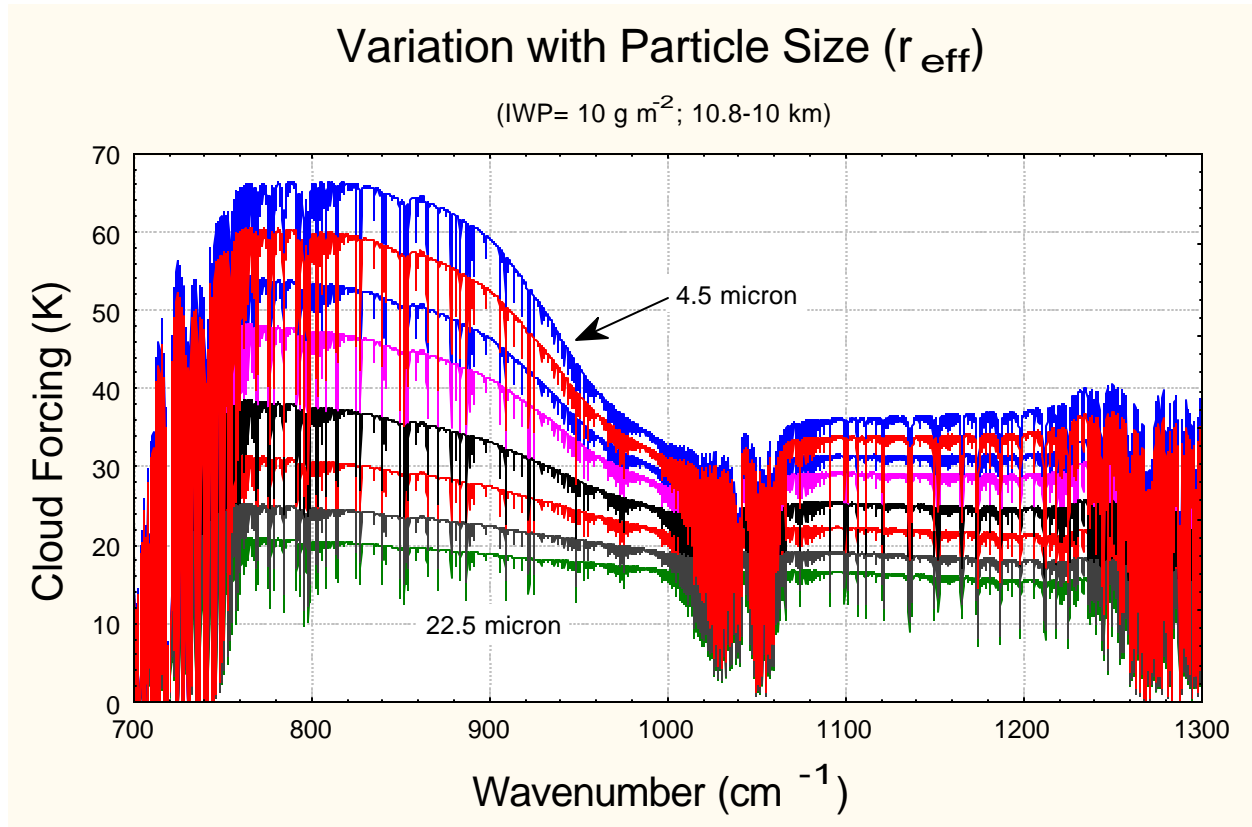


Figure 1a. The sensitivity of high spectral resolution observations to variations in cloud particle effective radius. Cloud forcing represents the brightness temperature difference between a clear and a cloudy sky calculation. Eight different effective radii are assumed, they are (from the top curve to the bottom) 4.5, 6.0, 7.5, 9.0, 12.0, 15.0, 18.75, and 22.5 μm . The cloud has a constant IWP of 10 g m^{-2} and a cloud top altitude of 10.8 km.

b

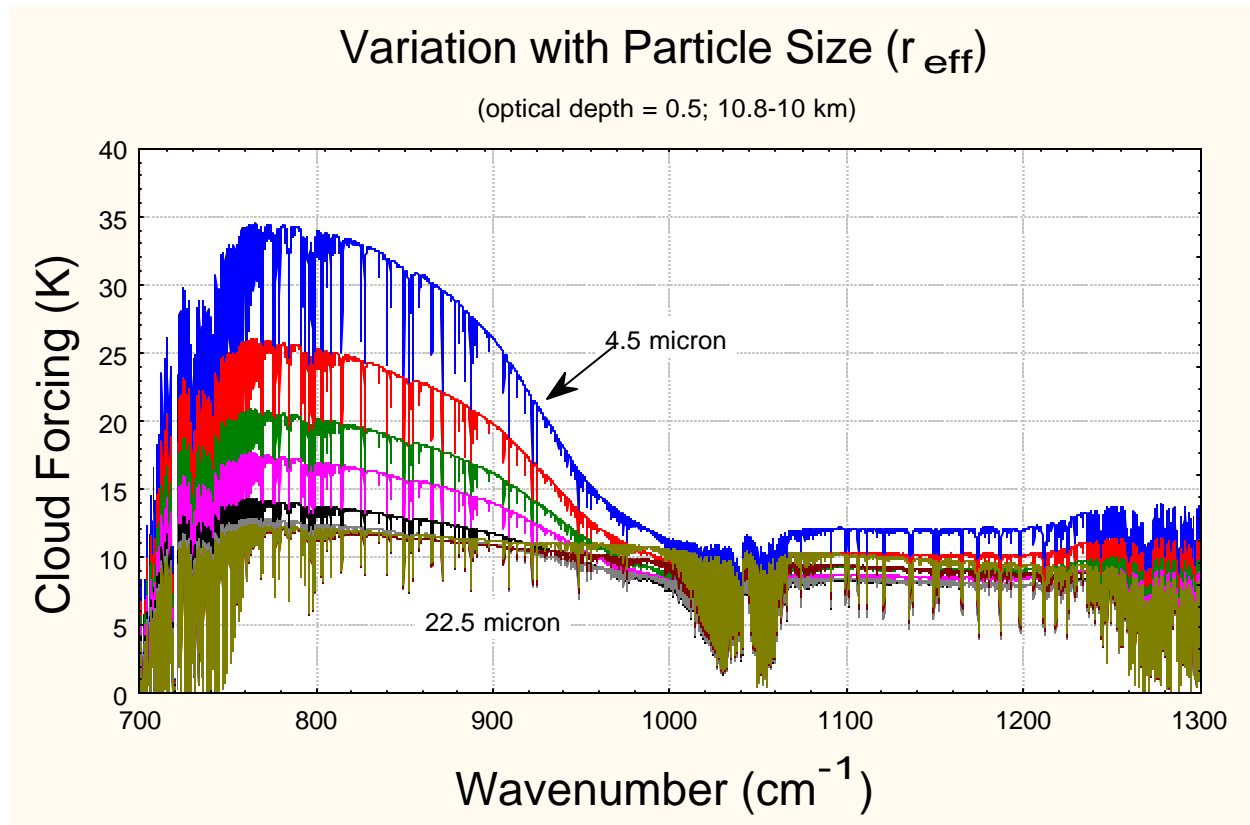


Figure 1b. The sensitivity of high spectral resolution observations to variations in cloud particle effective radius. Cloud forcing represents the brightness temperature difference between a clear and a cloudy sky calculation. Six different effective radii are assumed, they are (from the top curve to the bottom) 4.5, 6.0, 7.5, 9.0, 12.0, 15.0, 18.75, and 22.5 μm . The cloud has a constant optical depth at 1000 cm^{-1} of 0.5 and the cloud top altitude is 10.8 km.

Variation with Ice Water Path

($r_{\text{eff}}=7.5$ micron; Cloud at 10.8-10 km)

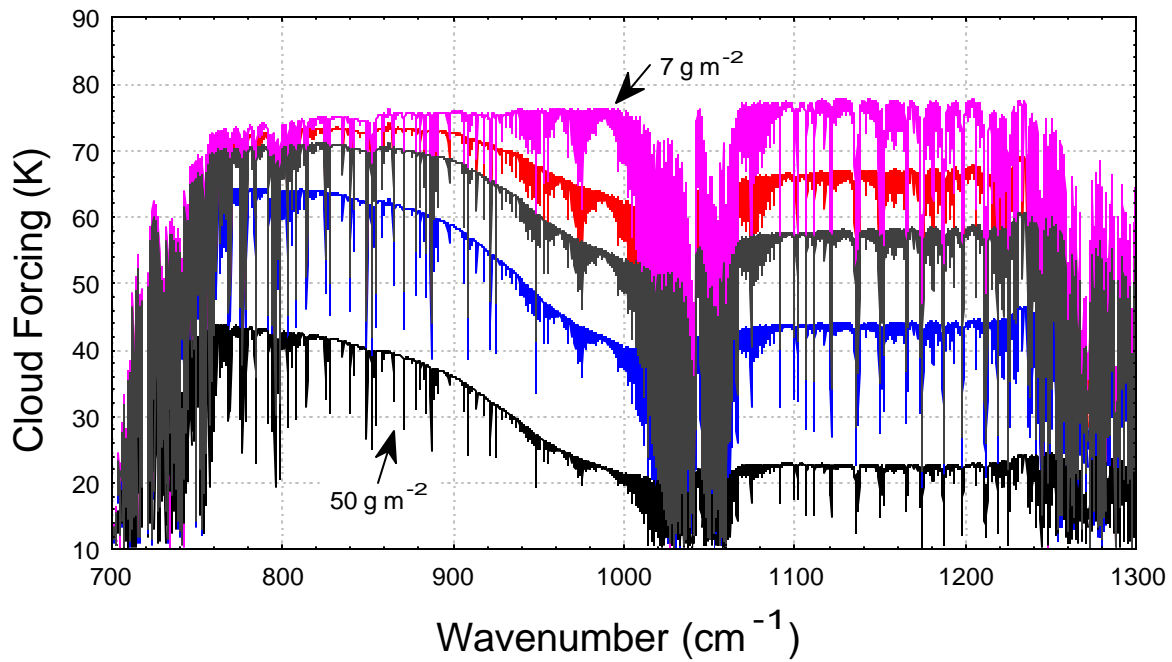


Figure 2. Cloud forcing as a function of wavenumber for 5 different IWPs: 50, 30, 22.5, 15 and 7.0 g m^{-2} (from top to bottom). The clouds have the same r_{eff} of 7.5 μm , a cloud top altitude of 10.8 km, and a thickness of 0.8 km.

Error due to wrong Cloud Altitude

(Cloud - 11.1-10.0 km; $r_{\text{eff}}=30$ micron; True IWP= 20 g m^{-2})

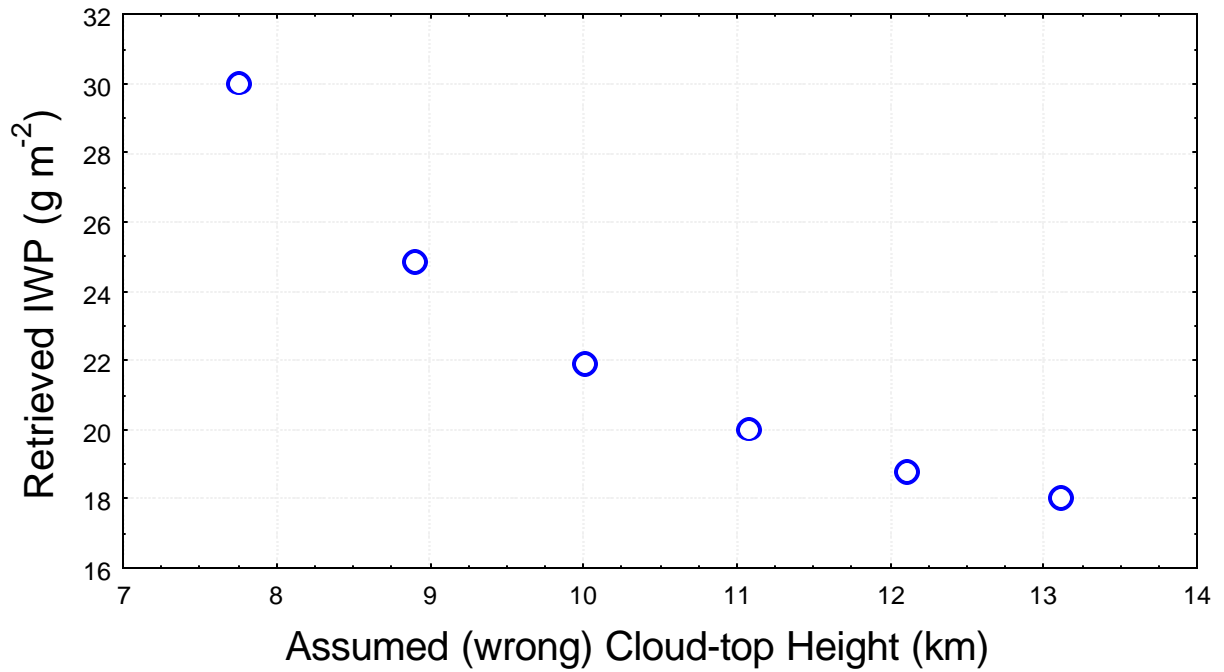


Figure 3. Differences in retrieved IWP if the cloud-top altitude is incorrectly assigned during the retrieval. The ice cloud has an IWP of 20 gm^{-2} , an effective radius of $30 \mu\text{m}$ and exists between 11.1 and 10.0 km.

Variation with Cloud Base Altitude

(IWP= 10 g m^{-2} ; $r_{\text{eff}} = 10.5 \text{ micron}$; CT= 13.12 km)

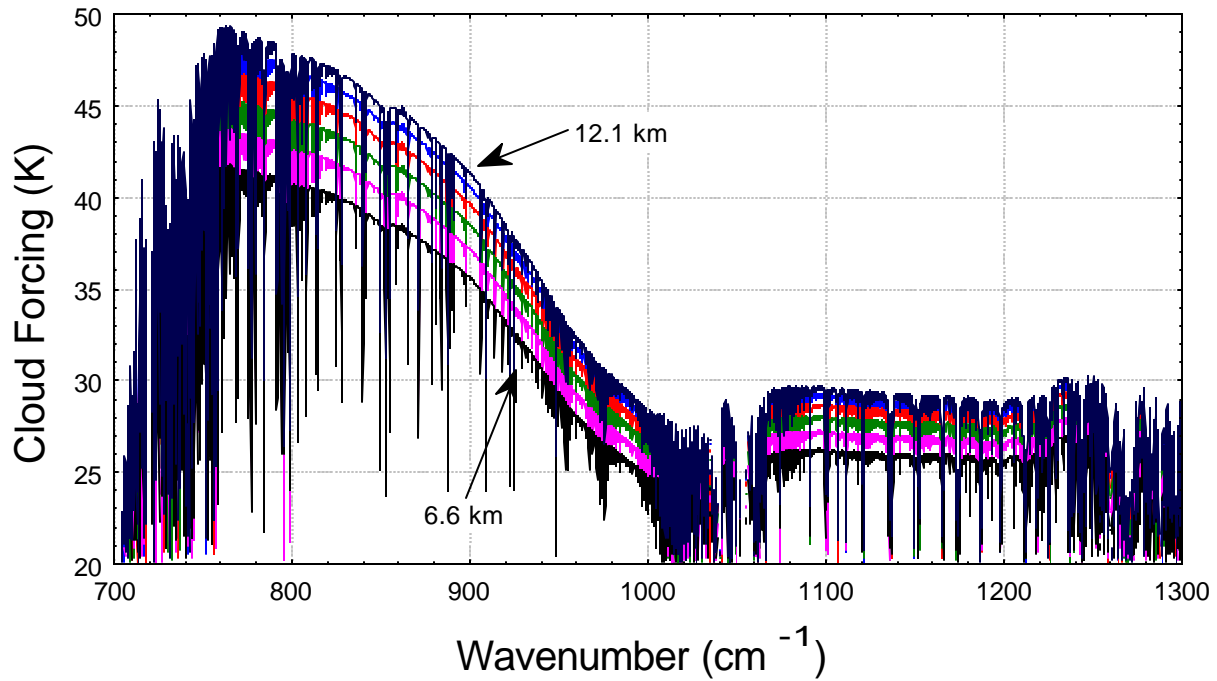


Figure 4. Cloud forcing as a function of wavenumber for different cloud base altitudes of 12.1, 11.1, 10.0, 8.9 and 7.8 and 6.6 km (from top to bottom). The cloud has a constant IWP of 10 gm^{-2} and consisting of ice particles of effective radius of $10.5 \text{ }\mu\text{m}$; the cloud top altitude is 13.1 km .

Multi-layer Cloud Condition

(Cirrus 11.1-10.0 km; $\epsilon_{\text{eff}}=7.5$; LWP=30 g m⁻²; $r_{\text{eff}}=20$ micron, DZ=1)

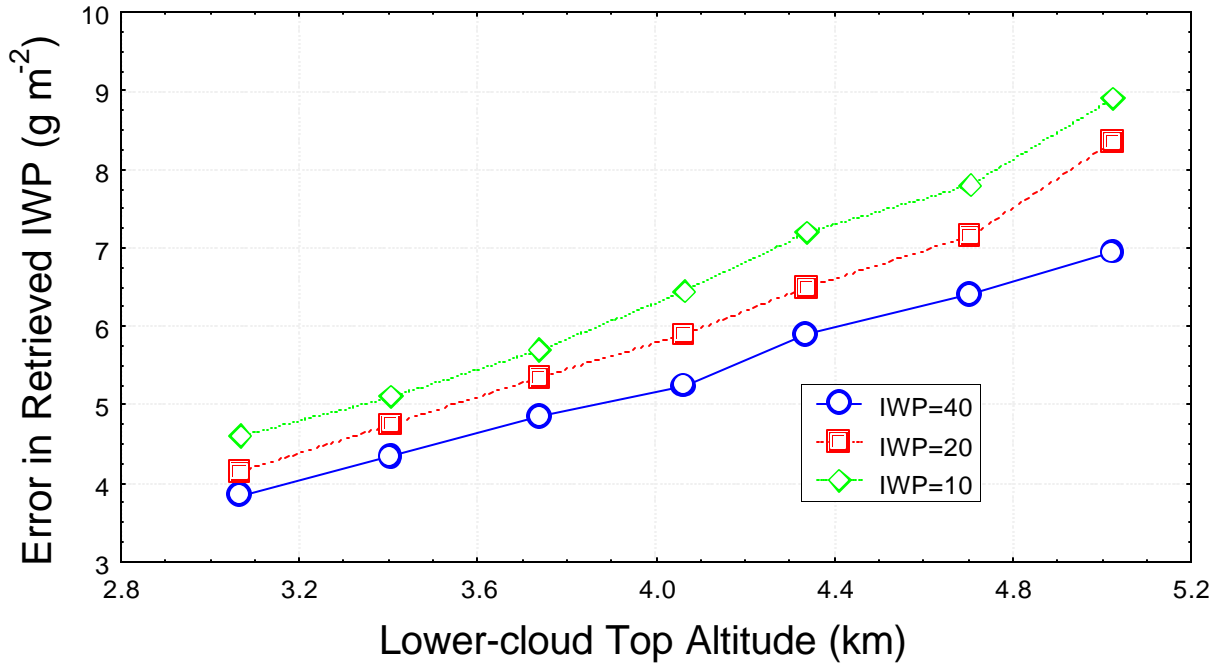


Figure 5. Errors in retrieved IWP for a multi-layered cloud condition if a single 1 km thick water cloud layer is assumed. The cirrus cloud contains ice particles of effective radius 7.5 μm and is between 11.1 and 10.0 km. The lower water cloud is approximately 1 km thick at altitudes ranging from 3.1 to 5.0 km and has an LWP of 30 g m⁻² and an effective particle radius of 20 μm . The retrieved errors are shown for three cirrus IWP conditions, 40, 20, and 10 g m⁻².

Two layer cloud with different r_{eff}

(IWP = 5 g m^{-2} for each layer; Cloud 11-8.9 km)

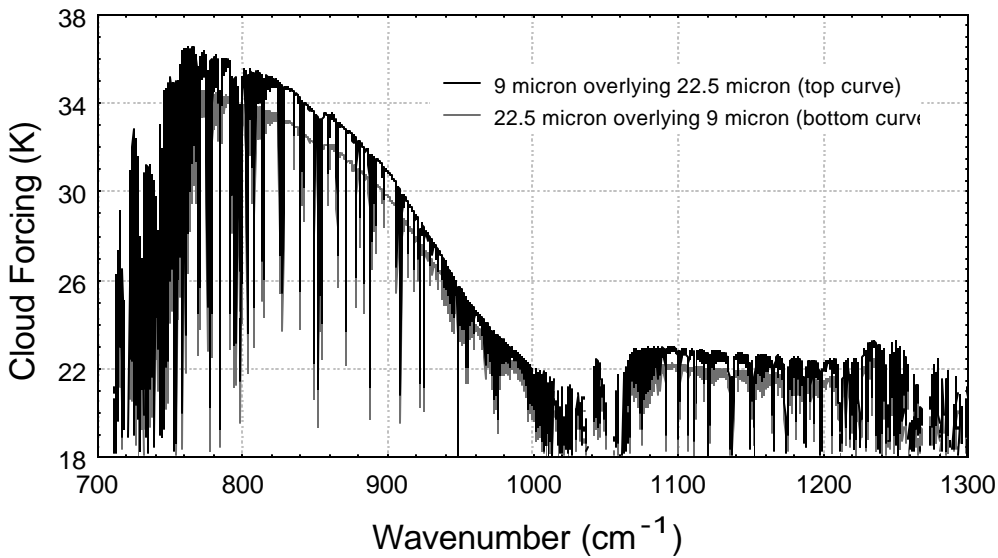


Figure 6. The sensitivity of high spectral resolution observations to variations in the vertical distribution of effective radius. In the top curve the upper cloud layer has an effective particle radius of $9.0 \mu\text{m}$ and the lower has an effective particle radius of $22.5 \mu\text{m}$. The particle sizes are reversed in the lower curve. Cloud forcing represents the brightness temperature difference between a clear and a cloudy sky calculation. The cloud has a constant IWP of 10 gm^{-2} and lies between 11.1 and 8.9 km.

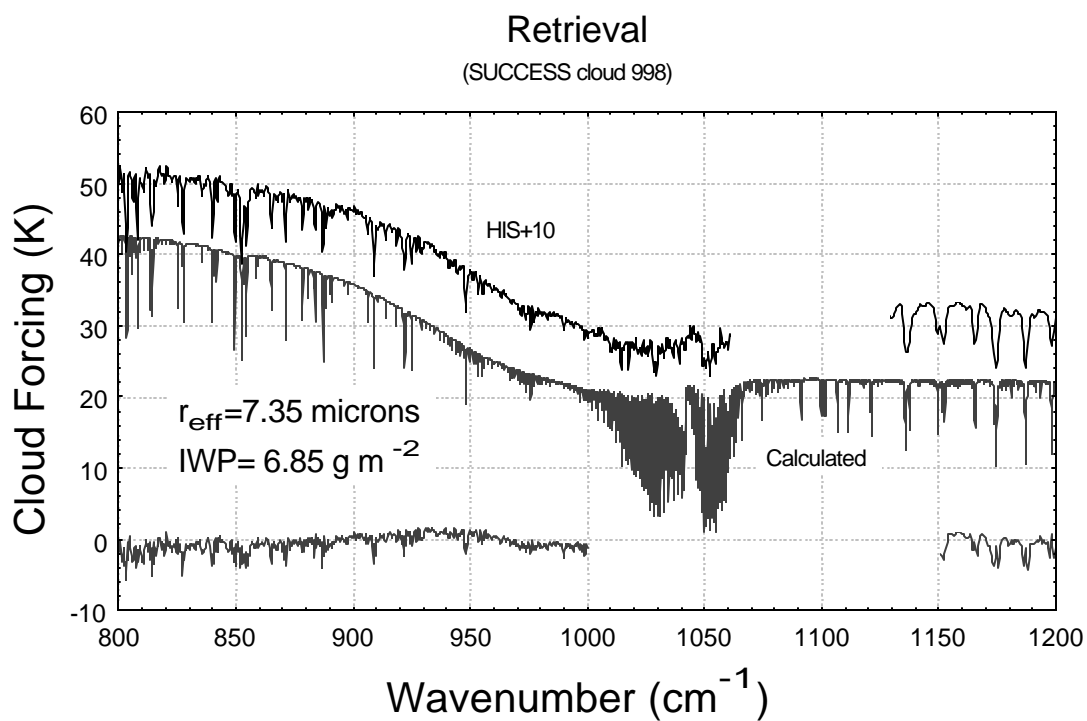


Figure 7. Cloud forcing as a function of wavenumber for a HIS observed spectrum during the SUCCESS experiment and results from a DISORT calculation with an effective radius of $7.35 \mu\text{m}$ and an IWP of 6.85 g m^{-2} . Shown are the full calculated spectra, the HIS observed spectra, and the difference spectra (at the HIS resolution) for those wavenumbers used in the fitting procedure.

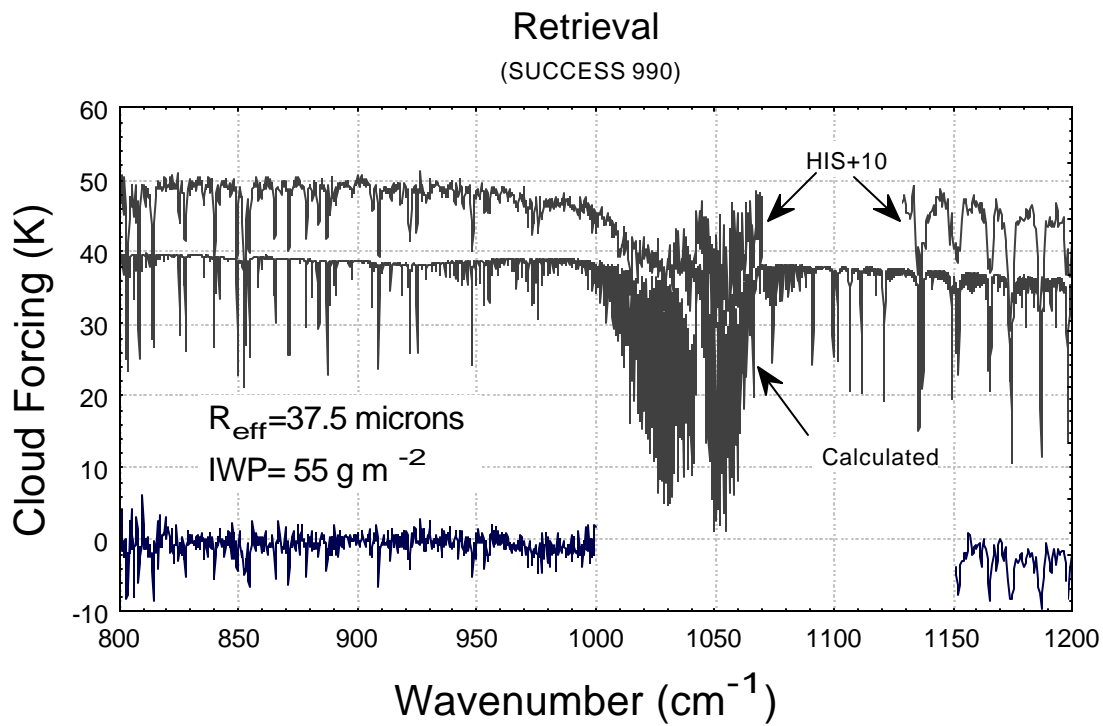


Figure 8. Cloud forcing as a function of wavenumber for a HIS observed spectrum during the SUCCESS experiment and results from a DISORT calculation with an effective radius of $37.5 \mu\text{m}$ and an IWP of 55 g m^{-2} . Shown are the full calculated spectra, the HIS observed spectra, and the difference spectra (at the HIS resolution) for those wavenumbers used in the fitting procedure.

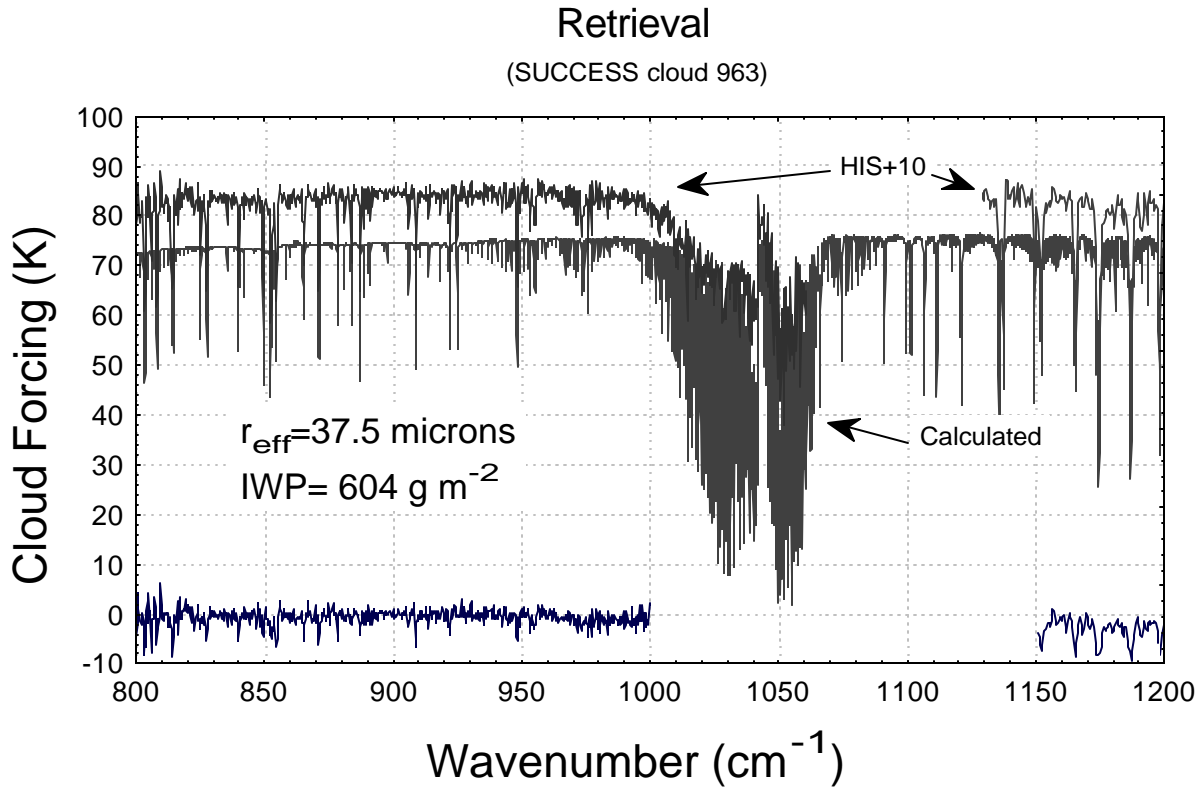


Figure 9. Cloud forcing as a function of wavenumber for a HIS observed spectrum during the SUCCESS experiment and results from a DISORT calculation with an effective radius of $37.5 \mu\text{m}$ and an IWP of 604 gm^{-2} . Shown are the full calculated spectra, the HIS observed spectra, and the difference spectra (at the HIS resolution) for those wavenumbers used in the fitting procedure.